THE ASTROPHYSICAL JOURNAL, 556:421–431, 2001 July 20

ON-THE-DISK DEVELOPMENT OF THE HALO CORONAL MASS EJECTION ON 1998 MAY 2

S. POHJOLAINEN,[1,2] D. MAIA,[1] M. PICK,[1] N. VILMER,[1] J. I. KHAN,[3,4] W. OTRUBA,[5] A. WARMUTH,[5] A. BENZ,[6] C. ALISSANDRAKIS,[7] AND B. J. THOMPSON[8]

Received 2000 November 11; accepted 2001 March 12

ABSTRACT

A halo coronal mass ejection (CME) was observed at 15:03 UT on 1998 May 2 by the *Solar and Heliospheric Observatory* Large-Angle Spectrometric Coronagraph. The observation of the CME was preceded by a major soft X-ray flare in NOAA Active Region 8210, characterized by a delta spot magnetic configuration and some activity in region 8214. A large transequatorial interconnecting loop (TIL) seen in the soft X-rays connected AR 8210 to a faint magnetic field region in the periphery of region 8214. Smaller loop systems were also connecting AR 8210 to other fainter bipolar magnetic structures, the interconnecting loop (IL) east of AR 8210 being one of the most visible. We present here a multiwavelength analysis of the large- and small-scale coronal structures associated with the development of the flare and of the CME, with emphasis placed on radio-imaging data. In the early phases of the flare, the radio emission sources traced the propagation paths of electrons along the TIL and the IL, which are accelerated in the vicinity of AR 8210. Furthermore, jetlike flows were observed in soft X-rays and in Hα in these directions. Significantly, the TIL and IL loop systems disappeared at least partially after the CME. An EUV Imaging Telescope (EIT) dimming region of similar size and shape to the soft X-ray TIL, but noticeably offset from it, was also observed. During the "flash" phase of the flare, new radio sources appeared, presenting signatures of destabilization and reconnection at discrete locations of the connecting loops. We interpret these as possible signatures of the CME liftoff on the disk. An Hα Moreton wave (blast wave) and an "EIT wave" were also observed, originating from the flaring AR 8210. The signatures in radio, after the wave propagated high into the corona, include type II–like emissions in the spectra. The radio images link these emissions to fast-moving sources, presumably formed at locations where the blast wave encounters magnetic structures. The opening of the CME magnetic field is revealed by the radio observations, which show large and expanding moving sources overlying the later-seen EIT dimming region.

Subject headings: Sun: corona — Sun: coronal mass ejections (CMEs) — Sun: flares — Sun: radio radiation — Sun: UV radiation — Sun: X-rays, gamma rays

On-line material: color figure

1. INTRODUCTION

"Halo" coronal mass ejections (CMEs) appear as diffuse clouds that surround the solar disk in white-light coronagraph images. Halo CMEs that originate on the visible solar hemisphere represent mass ejections that are directed toward the Earth and have therefore been found to be connected with geomagnetic disturbances and changes in the solar wind flow (see, e.g., Howard et al. 1982; Hudson et al. 1998; Sheeley et al. 1999; Torsti et al. 1998). Soft X-ray and EUV "dimmings" (interpreted as signatures of mass loss) are sometimes observed as the direct signature of eruptive events (including flares and/or CMEs) on the solar disk (Sterling & Hudson 1997; Thompson et al. 1998, 2000a; Zarro et al. 1999). Moreton-Ramsey waves ("flare waves") in Hα (Moreton & Ramsey 1960; Moreton 1960) and "EIT waves" observed by the EUV Imaging Telescope (EIT) as their possible coronal counterpart (Thompson et al. 1999, 2000b), have been observed originating from the vicinity of active regions and erupting quiescent filaments and have been suggested to be associated with filament eruptions, flares, and CMEs.

Flares and radio emission at metric wavelengths have often—but not always—been observed in association with CMEs (see, e.g., the review by Cliver, Webb, & Howard 1999). Recent results suggest that metric type II emission could be associated with blast waves driven by fast, short-lived X-ray ejecta from the flare region (Gopalswamy et al. 1998; Klein et al. 1999), but there is also some evidence for weak metric radio bursts associated with the leading edges of CMEs (Maia et al. 2000) as possible counterparts to interplanetary type II bursts that are associated with CMEs (Cane, Sheeley, & Howard 1987).

Most CME studies that have included radio-imaging observations have been of limb events. For example, Maia et al. (1999) showed the rapid development of the latitudinal extent of radio-emitting sources in connection with that of the CME and, moreover, they showed the involvement of multipolar magnetic systems as well as a series of loop system interactions leading to the opening of the coronal magnetic field. In contrast, we present here a detailed analysis of one disk event that was associated with a halo CME using coordinated observations from various ground- and space-based instruments, including, in particular, radio-imaging observations.

[1] Observatoire de Paris, UMR 8645, DASOP, Section de Meudon, Place Jules Janssen, Meudon Cedex, F-92195 Meudon, France.
[2] Tuorla Observatory, Väisäläntie 20, FIN-21500 Piikkiö, Finland; spo@astro.utu.fi.
[3] Mullard Space Science Laboratory, University College London, Holmbury Street Mary, Surrey, RH5 6NTUK.
[4] Institute of Space and Astronautical Science, 3-1-1 Yoshinodai, Sagamihara, Kanagawa 229-8510, Japan.
[5] Sonnenobservatorium Kanzelhöhe, A-9521 Treffen, Austria.
[6] ETH Zurich Institute of Astronomy, ETH-Zentrtum, CH-8092 Zürich, Switzerland.
[7] University of Ioannina, GR-45110 Ioannina, Greece.
[8] Space Applications Corporation, NASA Goddard Space Flight Center, Greenbelt, MD.

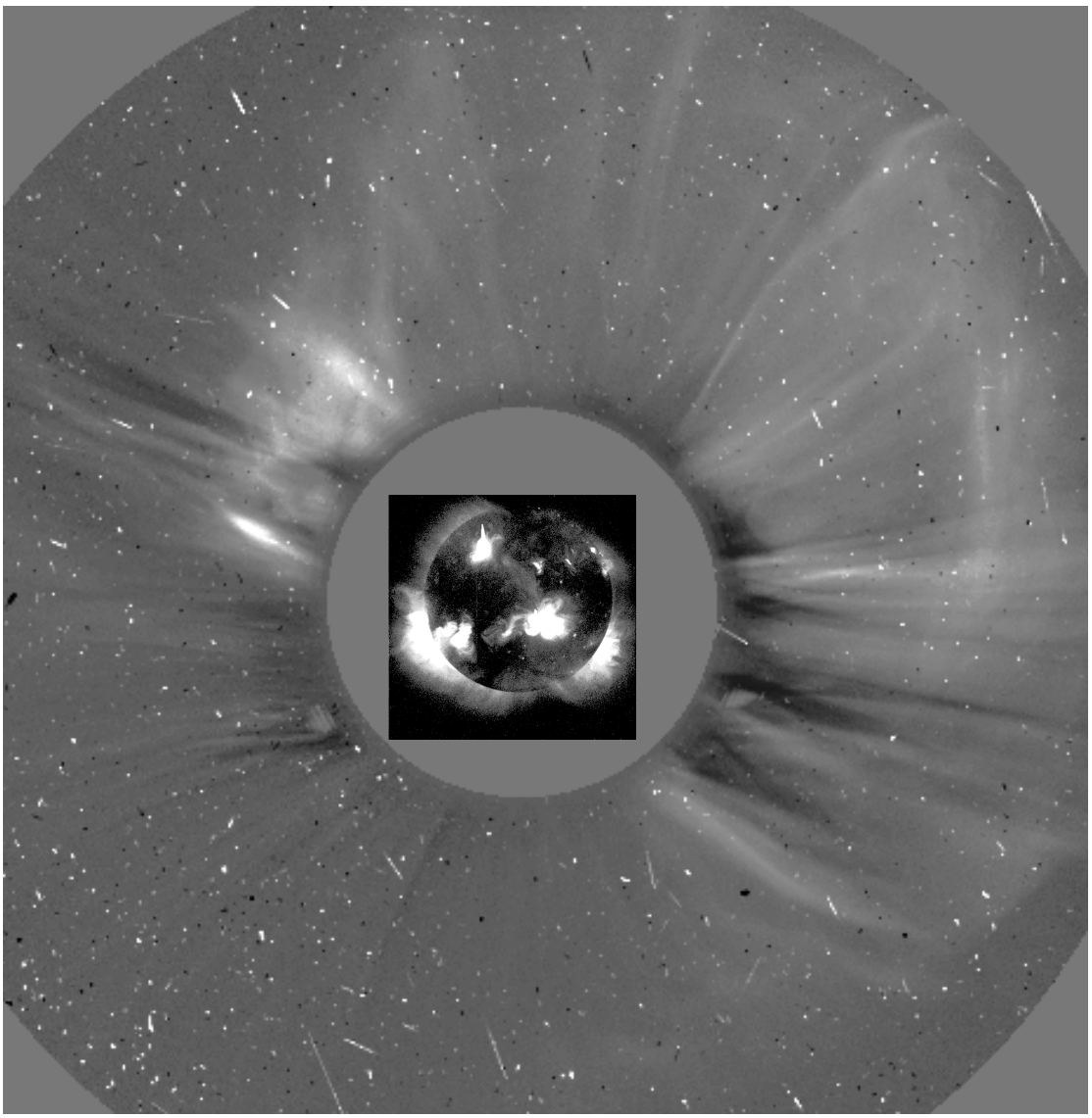

FIG. 1.—*SOHO* LASCO C2 difference image at 15:03–14:06 UT showing the halo CME on 1998 May 2. The bright pixels in the LASCO image are particle hits associated with the CME. Superposed is the preflare full-disk soft X-ray image of the Sun (*Yohkoh* SXT) at 13:26 UT. [*See the electronic edition of the Journal for a color version of this figure.*]

Preliminary studies of the 1998 May 2 event have been carried out by Pick et al. (1999), Pohjolainen, Khan, & Vilmer (1999), and Zharkova & Kosovichev (1999). Furthermore, Leblanc et al. (2000) have analyzed the interplanetary effects of the event.

In § 2 of this paper we describe the instruments briefly and present an overview of the observations. In § 3 we describe the observations in detail in separate sections: first, the soft X-ray observations, then the Hα observations, the EUV observations, the radio spectral data, and finally, the radio-imaging data. In § 4 we discuss the observations and draw conclusions.

2. INSTRUMENTS AND A SUMMARY OF OBSERVATIONS

In this study we concentrate on analyzing the Hα, X-ray, UV, and radio signatures as seen on the solar disk during the development of the halo CME on 1998 May 2. For this study, we use *Solar and Heliospheric Observatory* (*SOHO*; Domingo, Fleck, & Poland 1995) Large-Angle Spectrometric Coronagraph (LASCO; Brueckner et al. 1995) images in white light, *SOHO* EIT (Delaboudinière et al. 1995) images in the EUV, *Yohkoh* (Ogawara et al. 1991) soft x-ray telescope (SXT; Tsuneta et al. 1991) images in soft X-rays, *Yohkoh* Hard X-Ray Telescope (HXT; Kosugi et al. 1991) images in hard X-rays, Sonnenobservatorium Kanzelhöhe (Messerotti et al. 1999) and SOONSPOT network images in Hα, and Nancay Radioheliograph (Kerdraon & Delouis 1997) images at decimetric/metric radio wavelengths. In addition, we use the whole-Sun soft X-ray flux from the *GOES* satellites and the radio spectral data at decimetric/metric radio wavelengths from the Phoenix-2 at Zürich (Messmer, Benz, & Monstein 1999) and Artemis-IV in Greece (Maroulis et al. 1997).

A halo CME was observed by the *SOHO* LASCO C2 coronagraph at 15:03 UT on 1998 May 2. An estimate of the CME speed could be made with the help of the previous LASCO image at 14:06 UT, and it was estimated to be over 1039 km s^{-1}. A composite image of a *Yohkoh* SXT full-disk

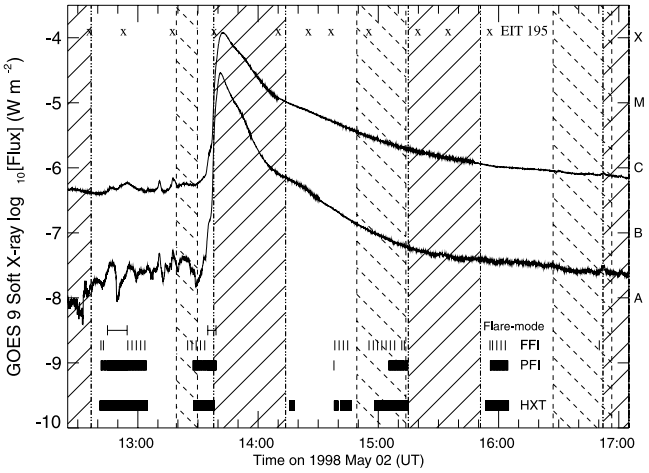

FIG. 2.—*GOES 9* soft X-ray flux at 1–8 Å (*higher flux curve*) and at 0.5–4 Å (*lower flux curve*) on 1998 May 2. Superposed on these are hatched areas representing the intervals of *Yohkoh* satellite night and dashed hatched areas representing South Atlantic Anomaly intervals (high-voltage detectors turned off). Small vertical tic marks indicate the times of *Yohkoh* SXT full-frame images (FFI), partial frame images (PFI), and HXT observing times. *SOHO* EIT 195 Å observing times are marked with crosses. The Kanzelhöhe Hα image cadence is 1 minute, while the Nancay radio image cadence is 0.5 s at each frequency.

soft X-ray image at 13:26 UT and a *SOHO* LASCO C2 difference image at 15:03–14:06 UT are presented in Figure 1.

The *GOES 9* full-Sun soft X-ray flux curves are presented in Figure 2. A *GOES* X1.1-class flare was observed in active region 8210 during 13:30–16:00 UT. A *GOES* B6.5-class flare was observed in AR 8214 during 13:14–13:19 UT. The observing times of the *SOHO* EIT and the two *Yohkoh* instruments are marked on the plot. *Yohkoh* nighttime set in around 13:37 UT, and observations started again well after 14 UT. The *SOHO* EIT took 195 Å images every 20 minutes during the flare, around 13:19, 13:41, and 14:10 UT. Hα data from the SOONSPOT network and Kanzelhöhe are available with 1 minute image cadence.

The Phoenix-2 spectrograph at ETH in Zürich and the Artemis-IV spectrograph in Greece recorded the whole event from meter to centimeter wavelengths. The Nancay Radioheliograph imaging observations were carried out at five decimetric/metric frequencies (164, 236, 327, 410, and 432 MHz) with a 0.5 s image cadence at each frequency.

3. OBSERVATIONS

3.1. *X-Ray Emission*

The *Yohkoh* SXT soft X-ray image in Figure 3*a* shows two active regions, NOAA AR 8210 (S15°, W15°) and AR 8214 (N25°, E25°) on the disk. A system of transequatorial interconnecting loops (TILs) is observed connecting AR 8210 to the peripheries of AR 8214 in the northern hemisphere. In the vicinity of the TIL, there are smaller scale soft X-ray features that were not classified as sunspot regions by NOAA (e.g., the region AB) but that are visible in the magnetograms as small bipolar regions. An interconnecting loop (IL) in soft X-rays connected AR 8210 to a region east of it (region AC).

The major *GOES* X-class soft X-ray flare in the southern AR 8210 first showed a flux rise around 13:30 UT. *Yohkoh* imaging was triggered into flare mode at 13:34:06 UT. In the rising phase of the soft X-ray flare—*GOES* maximum was at 13:42 UT—two spraylike flows, J1 and J2, were seen until *Yohkoh* night set in around 13:37:30 UT. The flow features observed in Hα and in soft X-rays are presented in Figures 3*a* and 3*b*, with locations in respect with the TIL and IL. No definite speeds for these sprays could be calculated since there were no clear leading edges in the flows. The spray J1 was fainter than the other and seemed to

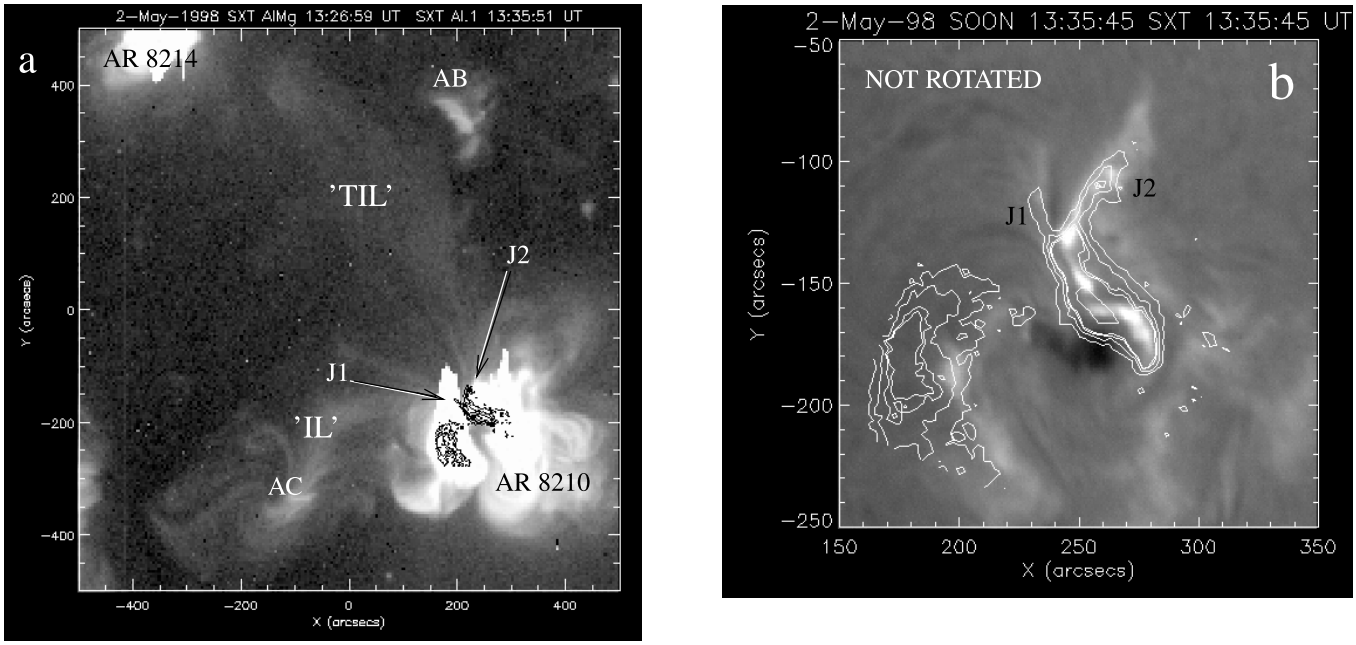

FIG. 3.—(*a*) *Yohkoh* SXT Al-Mg large field of view at 13:26:59 UT (in gray scale with long exposure time; saturated areas are seen in white) with the SXT Al.1 contours at 13:35:51 UT superposed showing the flaring region inside AR 8210. The sunspot regions AR 8210 (S15°, W15°) and AR 8214 (N25°, E22°) were connected by a TIL, and the smaller region AC was connected to AR 8210 by an IL. Also, other small regions were seen on the disk; the one near the TIL is labeled "AB." The arrows point to the flow directions of the flare, labeled "J1" and "J2." (*b*) SOONSPOT Hα image of the flare region at 13:35:45 UT superposed with *Yohkoh* SXT contours at 13:35:45 UT.

follow a short loop along the IL, while J2 was more intense and was directed toward the TIL.

Yohkoh HXT light curves show that the hard X-ray emission at the lowest energy channels (14–53 keV) started to rise around the time when the flare mode was triggered. During the intense emission phase (just before satellite night set in), the strongest component of hard X-ray emission at 33–53 keV elongated toward the southwest.

In the next full-frame *Yohkoh* SXT image after the flare, the TIL had mostly disappeared, and most of the smaller IL toward region AC had disappeared as well. These SXT dimming regions are presented in the difference image in Figure 4.

3.2. Hα *Observations*

The Hα flare, first observed at 13:34:38 UT, is described in detail by Warmuth et al. (2000). An Hα wave (Moreton-Ramsey wave) was first observed in the image at 13:38:57 UT heading north and northwest from the active region. We estimate the start time of the wave to be around 13:38:00 UT. In the next image at 13:39:47 UT, the wave front was split into two parts: one moving north at 790 km s^{-1} and the other moving northwest at 630 km s^{-1}. It seems that the latter front had been slowed down by crossing an Hα structure (Warmuth et al. 2000). Later on, the speeds of both Hα wave fronts slowed down significantly to about 320 km s^{-1} at 13:44:57 UT. The temporal evolution of the Hα wave front is presented in Figure 5.

3.3. *SOHO EIT Observations*

An EIT wave was observed in the *SOHO* EIT 13:41–13:19 UT difference image. Figure 6 presents this difference image together with the positions of the Hα wave fronts. The EIT image cadence was too low to measure the speed of the EIT wave disturbance accurately. However, a very rough lower limit of 340 km s^{-1} is implied by comparing the image where the EIT wave was seen at 13:41 UT and assuming that the wave started at the flare site at the start of the flare (both questionable assumptions). Moreover, since the Hα and EIT wave fronts are nearly cospatial around 13:41 UT, we suggest that the actual EIT wave speed is much larger than the lower limit given here.

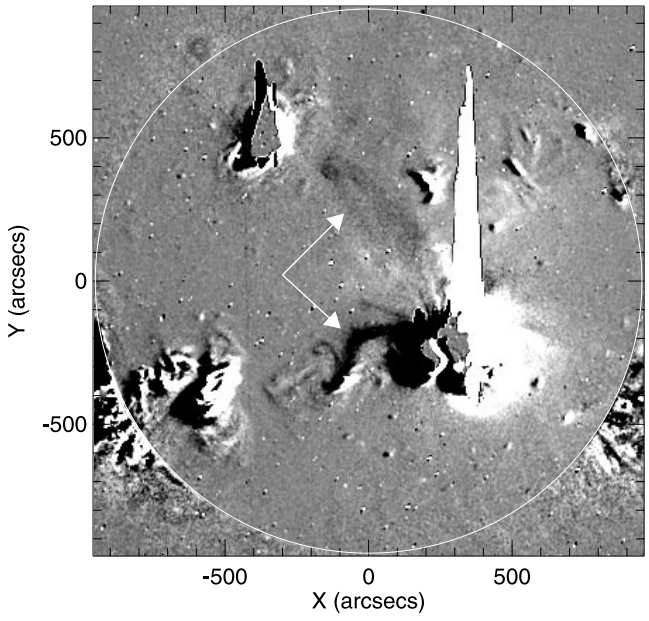

FIG. 4.—*Yohkoh* SXT difference image at 15:55:42–13:26:58 UT on 1998 May 2. Dark areas represent reduced brightness-depleted matter. The arrows point to the systems of loops that disappeared at least partially.

An "EIT dimming" region, also reported in Thompson et al. (2000a), was observed in the next EIT difference image pair at 14:10–13:41 UT, shown in Figure 7. The dimming persisted to some extent until at least 22:00 UT. The dimming region was located north of AR 8210. The Hα wave was observed to travel approximately along part of the region that dimmed.

3.4. *Radio Spectral Data*

Between 13:28 and 13:37 UT, the radio spectral data at decimetric/metric wavelengths showed pulsations and several type III and type III–like radio bursts. Similar type III activity in the preflash phase of flares has been reported by, e.g., Raoult et al. (1985). Some of the type III–like radio bursts at low frequencies were J-shaped (incomplete U-bursts). The one that occurred around 13:34:50 UT (in the preflash phase) had a turnover frequency near 150 MHz. A selected part of the spectra, from 13:33:30 to 13:53:30 UT at 115–700 MHz, is presented in Figure 8.

At 13:37:30 UT, an intense "radio flash" took place (see Fig. 9). By the radio flash phase we mean the sudden, very large increase in the radio and hard X-ray emission with an increase of the radio flux toward the high frequencies. At frequencies below 230 MHz, the emission drifted toward lower frequencies at a rate of about 15 MHz s^{-1}. This fast-drifting source is labeled "M0" in the spectral plots in Figures 8 and 9. Superimposed on this drifting emission were short, narrowband, type III–like bursts, including a J-burst at 13:37:51 UT with a turnover frequency near 120 MHz. After the fast-drift phase, some U-bursts were seen at narrow frequency ranges, for example, at 236 MHz at 13:38:48 UT. Some frequency-drifting bursts toward the higher frequencies were also observed after the flash onset phase (Fig. 9).

During 13:41–13:46 UT, several slower (relative to M0) frequency-drifting bursts were seen. These are labeled "M1," "M2," and "M3" in Figures 8 and 9. The drifts were about 1 MHz s^{-1}. Type II bursts usually have frequency drift rates in the 0.1–1.0 MHz s^{-1} range (Roberts 1959; Kundu 1965; Cliver et al. 1999). Also, the drifting features observed here did not show corresponding harmonic features. Thus, we refer to these features as type II–like bursts. If extrapolated toward higher frequencies, the radio spectra of M2 and M3 seem to indicate that the two sources may have a common start time around 13:42 UT, just below 300 MHz.

After 13:42 UT, an intense continuum source was formed at the 300–1400 MHz frequency range, which is marked "CONT" in Figure 9. After this continuum emission started, no type II–like emission sources were formed. After 14:10 UT and up to 15:00 UT, a strong prolonged radio continuum source was observed, seen in the Nancay flux curves in Figure 10.

3.5. *Radio-imaging Data*

Figure 10 shows the time evolution of the radio flux at four frequencies observed with the Nancay Radioheliograph. This illustrates in summary the signatures at decimetric/metric wavelengths of the full development of

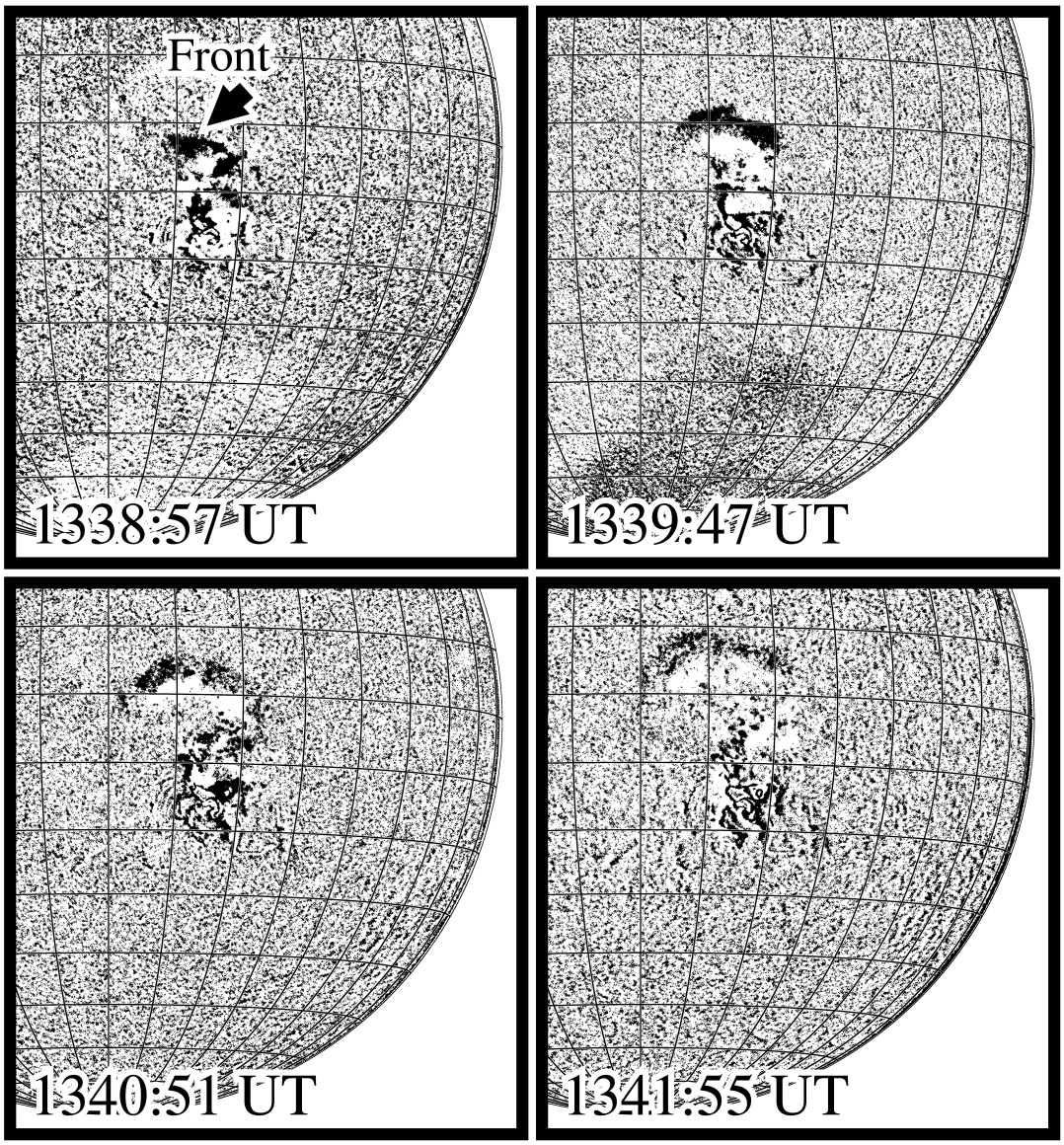

FIG. 5.—Running difference of Kanzelhöhe Hα images showing the moving Hα wave front (marked by an arrow in the first difference image)

the flare, shock wave, and CME, described in further detail below with radio-imaging data.

The type III bursts that were observed between 13:28 and 13:35 UT appeared near AR 8210, either on the north side of the active region or on the east side of the active region. The radio emission paths seemed to follow the magnetic features, tracing EUV and soft X-ray loops that were coming out of the active region. Around 13:35 UT, the locations of the radio emission sources at all Nancay observing frequencies traced large looplike structures—an example is shown in Figure 11—that linked the AR 8210 to the peripheries of AR 8214. This "radio sources' path" overlapped significantly with the TIL that was seen in soft X-rays. The location of the radio loop "leg" was over AR 8210. This indicates that the first nonthermal electrons were produced in the vicinity of AR 8210.

Between 13:37:10 and 13:38:45 UT (the flash phase clearly seen in the spectrum), a new radio source M0 was seen in the Nancay images on the west side of AR 8210 (Fig. 13). This westward source corresponds to the rapidly drifting spectral feature M0 in Figure 8. The spectral drift for M0 was about 15 MHz^{-1}. The source locations at 164 and 236 MHz are the same, which indicates accelerated electrons moving up roughly toward the Earth. The radio flux for the M0 source was very intense, and it probably swamped any radio emission coming from the transequatorial loop direction, if still produced.

Once the radio flux from the westward and the preexisting source diminished, new radio looplike structures were seen apparently connecting AR 8210 with the small diffuse region to the north (labeled "AB" in Fig. 3). The region AB was also seen as a faint bipolar region in the magnetograms. Examples of radio images at 13:38:48 UT (corresponding to the narrowband U-burst mentioned in the previous subsection) and at 13:39:13 UT (new illuminated looplike structures) at 236 MHz are presented in Figures 12*a* and 12*b*, respectively. Compared to Figure 11, the looplike structure at 13:38:48 UT is displaced toward the west and still shows some emission associated with M0. A large radio "arc" structure—which had a similar location as the pre-

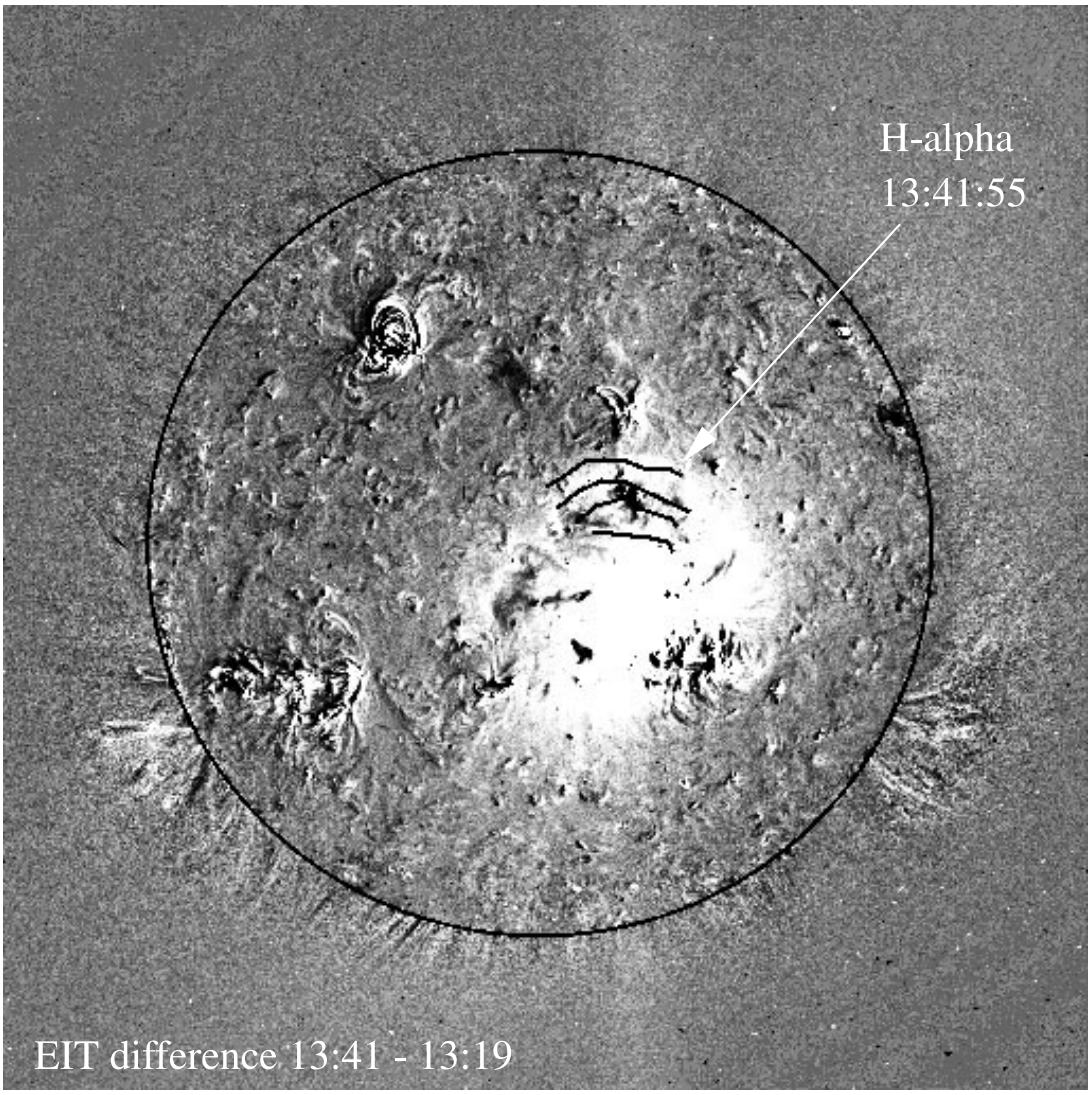

FIG. 6.—Positions of the Kanzelhöhe Hα wave fronts at 13:38:57, 13:39:47, 13:40:51, and 13:41:55 UT (*solid lines*) plotted over *SOHO* EIT difference image at 13:41:18–13:19 UT on 1998 May 2.

vious radio path at 13:35 UT roughly along the TIL—was formed around 13:40 UT and shown in Figure 12*c*. However, this one had a new source near the solar north pole.

Several short-duration moving radio sources were then observed on the solar disk between 13:41 and 13:45 UT. At the same time, several type II–like frequency-drifting sources (M1, M2, and M3) were seen in the spectra below 300 MHz (in Fig. 8). All the moving sources (M1–M3) and the western source M0 in the radio flash phase are presented in Figure 13. Spectral source M1 was seen in the radio images only at 164 MHz. Its speed could not be determined accurately, although the direction was northward. Source M2 was seen at 236 MHz and later at 164 MHz moving northeastward. It had a projected speed of about 830 km s^{-1}. Source M3 was seen at 236 MHz and later at 164 MHz moving toward the west limb. It had a projected speed of about 890 km s^{-1}. The spectral drifts for sources M1–M3 were approximately 1 MHz s^{-1}.

After 13:42 UT, the Nancay radio images showed an elongated source overlying the region connecting AR 8210 and region AB, and the source was seen moving slowly at 327 MHz with a projected speed of about 300 km s^{-1}. From 13:48 UT to around 13:53 UT, this radio emission source formed an arclike structure, which coincides with the coronal dimming region seen later in the *SOHO* EIT image at 14:10 UT. The radio arc at 13:48 UT was plotted over the EIT dimming region in Figure 7. After 14:10 UT, a strong and compact radio continuum source was seen over AR 8210. The flare evolution and the different radio signatures are summed up in a time line in Figure 14.

4. DISCUSSION

The purpose of this study was to analyze the Hα, X-ray, UV, and radio signatures associated with the disk flare and the early development of the halo CME on 1998 May 2. It must first be remembered that although many loops are seen inside the flaring region or linking the flaring active region to the peripheries of other active regions or to fainter bipolar regions on the solar disk, in X-ray observations by *Yohkoh* and in the EUV by *SOHO* EIT (while many more remain unseen by these instruments), the radio-imaging observations select and trace—via nonthermal radiation—only those loops or loop systems at different scales that

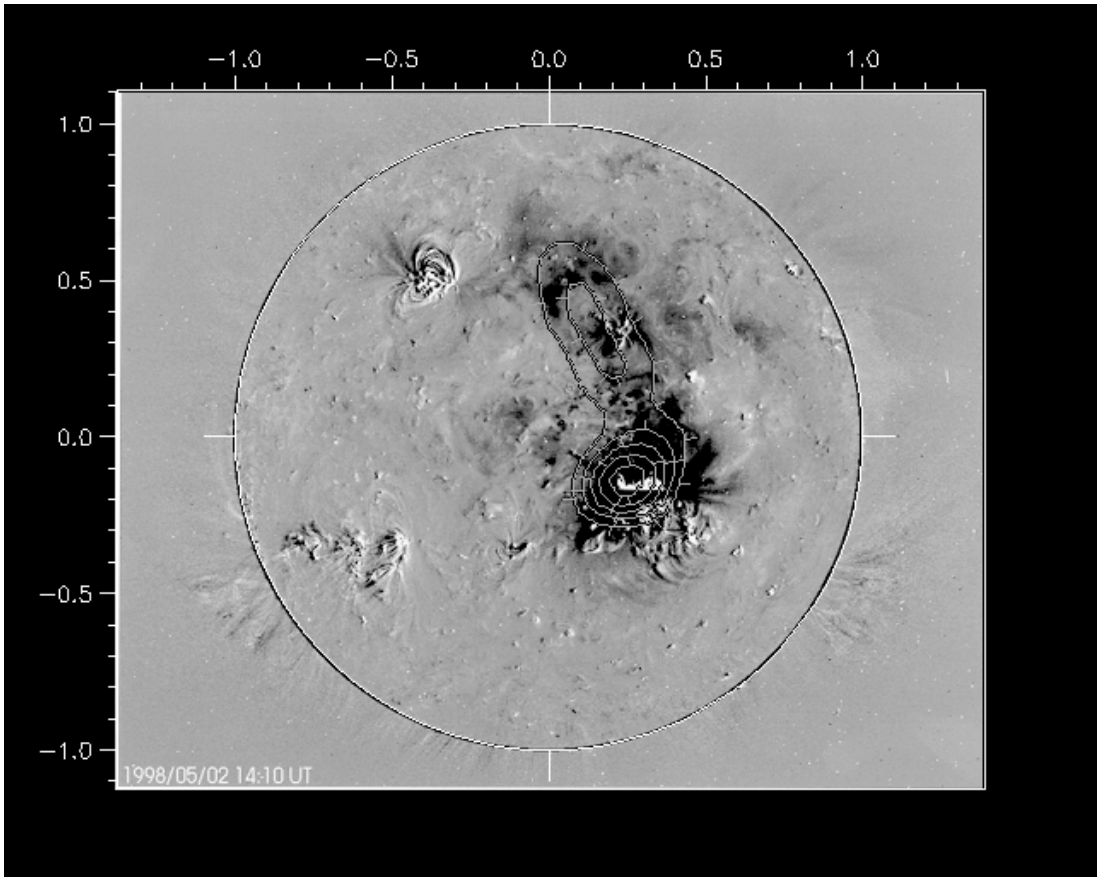

FIG. 7.—*SOHO* EIT 195 Å percentage difference image at 14:10–13:41 UT on 1998 May 2 showing the EIT dimming region position at 14:10 UT. The Nancay 236 MHz image at 13:48:21 UT is overplotted in contours. The figure axes are in solar radii. The moving continuum source was seen in the Nancay radio images during 13:43–13:53 UT. At the time of the EIT image (showing the dimming), this radio source had already disappeared.

have footpoints in the flaring active region and that actively contribute to the CME development. In particular, the TIL, observed between the flaring region AR 8210 and the fainter magnetic regions in the peripheries of AR 8214, seems to play a crucial role in the development of the 1998 May 2 CME as well as in the developments of three other CMEs occurring in a very similar magnetic configuration (Khan & Hudson 2000). In this case, the smaller IL and possibly the loop system connecting AR 8210 to the faint bipolar region AB also seem to take part in the CME development.

The first manifestations of activity seen at radio wavelengths are observed after 13:28 UT, which is well before

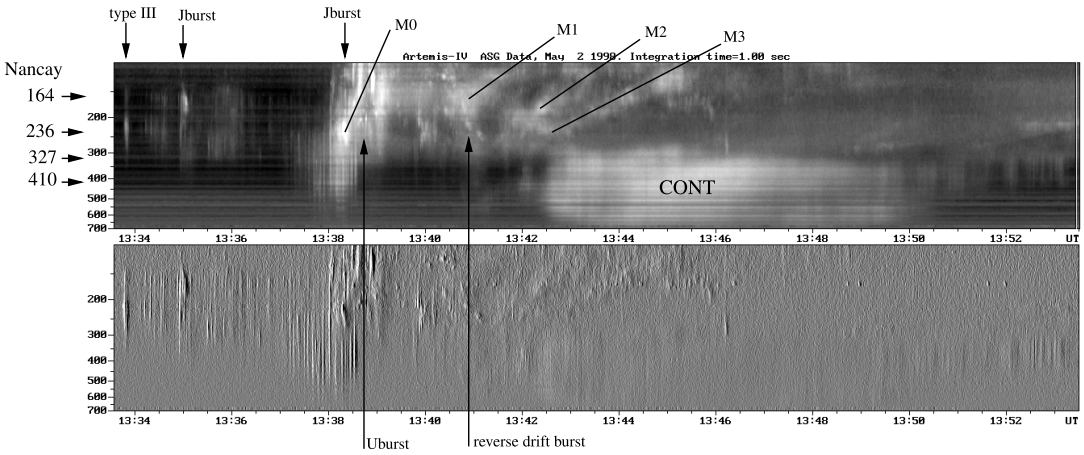

FIG. 8.—Artemis-IV spectra at 115–700 MHz at 13:33:30–13:53:30 UT. The lower panel shows the time derivative of the intensity. The Nancay imaging frequencies are marked on the left. The most intense type III bursts and J-bursts and one of the U-bursts (imaged in Fig. 12*a*) are marked with arrows. The spectral drifting sources are labeled "M0" for the one in the radio flash phase and "M1," "M2," and "M3" for the type II–like emission. One of the reverse drift bursts is also marked. The continuum emission source is labeled "CONT" (as in Fig. 9).

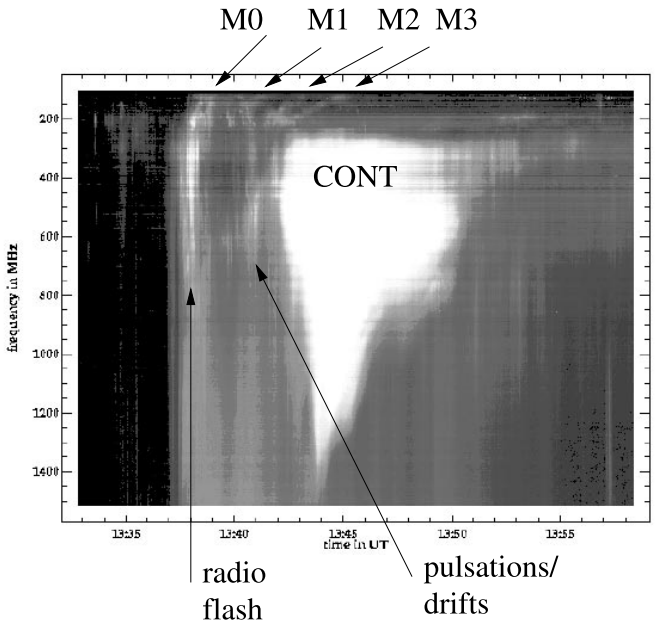

FIG. 9.—Phoenix-2 spectral plot from ETH Zürich at the frequency range 100–1500 MHz at 13:33–13:58 UT on 1998 May 2. The spectral plot shows how the emission in the radio flash phase extends to microwave frequencies. The pulsations and frequency-drifting bursts were observed between the radio flash phase and the strong continuum source (CONT).

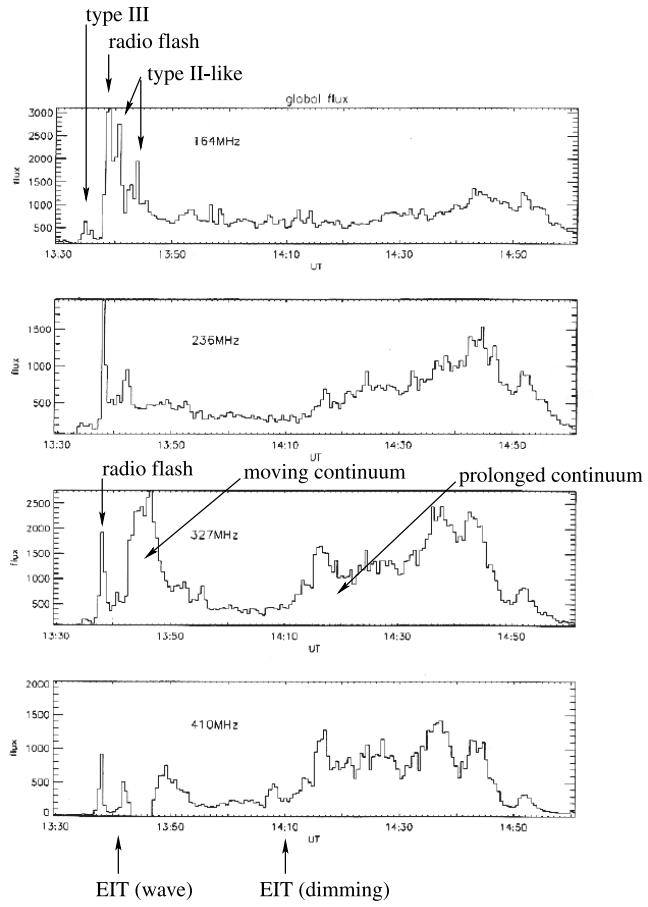

FIG. 10.—Nancay whole-Sun total flux at 164, 236, 327, and 410 MHz from 13:30 to 15:00 UT on 1998 May 2. The arrows mark the approximate start times of the strongest radio features. The *SOHO* EIT observing times are also marked in the plot.

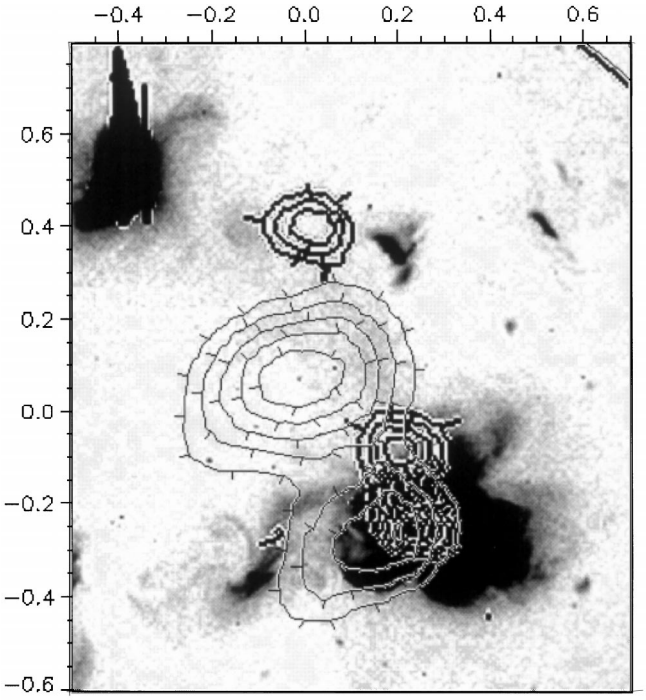

FIG. 11.—Nancay 327 MHz sources at 13:35:01 UT (*black contours*) and at 164 MHz at 13:35:14 UT (*gray contours*) over the *Yohkoh* SXT preflare image (*reversed colors*) at 13:26:59 UT on 1998 May 2. The axes units are solar radii. The lower frequencies were located in the middle part of the soft X-ray TIL and the higher frequencies near the TIL footpoints, indicating electron acceleration along the soft X-ray loop.

the onset of the radio flash phase around 13:37 UT. These type III bursts and J-bursts occur in the large transequatorial loop system and in the smaller interconnecting loops, where a small number of electrons accelerated in the vicinity of AR 8210 propagate and radiate radio waves. This early energy release—which can be interpreted as evidence for magnetic reconnection—is also shown in the Hα and soft X-ray observations of jetlike flows, closely coaligned with the TIL and IL directions. The first radiation of nonthermal electrons thus occurs within the TIL and IL loop systems—which at least partially disappear during or after the CME.

At radio wavelengths, the flash phase shows typical evolution with emission suddenly extending to high frequencies (at least up to 1.6 GHz) and a new radio source M0 appearing at decimetric/metric wavelengths. This explosive phase also corresponds to a displacement of the brightening in the active region, indicating that new energy release sites (i.e., newly activated magnetic features) were present. Similar appearances of new radio sources during the flare development have been reported previously (Raoult et al. 1985; Chupp et al. 1993; Trottet et al. 1998). In our event, the radio flash emission presents a fast spectral drift (15 MHz s^{-1}) at metric wavelengths below 230 MHz. Within this rapidly drifting emission, narrowband type III–like bursts and J-bursts are superposed. The decreasing turnover frequency of J-bursts (with respect to the preflash phase) indicates that electrons progressively have access to loops higher up in the solar atmosphere because of either the opening of large-scale fields in the vicinity of the TIL or

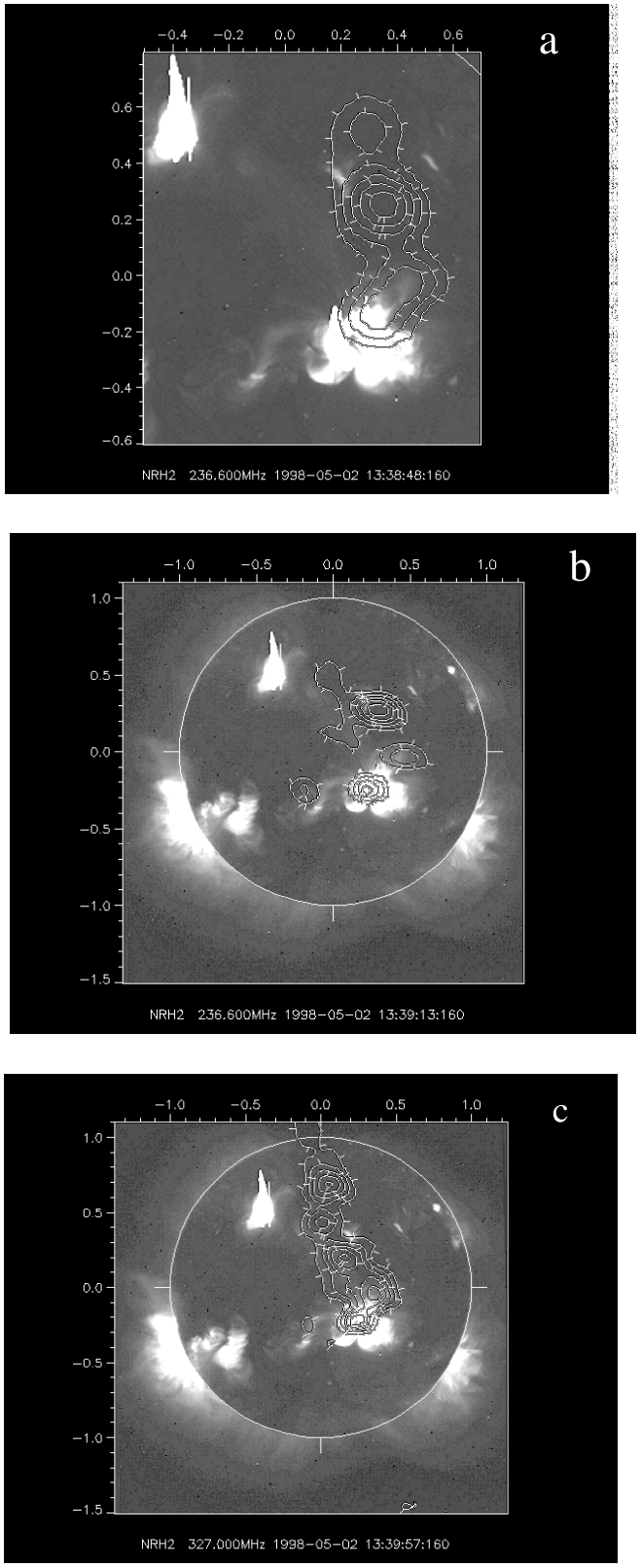

FIG. 12.—(*a*) Nancay 236 MHz sources at 13:38:48 UT (*contours*) plotted over the *Yohkoh* SXT image at 13:26:59 UT on 1998 May 2. The spectra shows a short narrowband U-burst at this time. (*b*) Nancay 236 MHz sources at 13:39:13 UT (*contours*) plotted over the *Yohkoh* SXT image at 13:26:59 UT on 1998 May 2. Illuminated looplike structures are seen in radio. (*c*) Nancay 327 MHz sources at 13:39:57 UT (*contours*) plotted over the *Yohkoh* SXT image at 13:26:59 UT on 1998 May 2. A large radio looplike structure is visible, similar to the one observed around 13:35 UT, but now with a new radio source near the solar north pole. The axes units are solar radii.

having access to new loop systems. This interpretation is also suggested by the displacement of the radio-illuminated arc system connecting AR 8210 and the small diffuse region above it and by its increased spatial extent.

About 1 minute after the flash phase, a Moreton Hα wave was observed propagating from the flare site with speeds around 630–790 km s^{-1} along different directions. The start of the Hα wave is estimated to be very close to the radio flash, around 13:38 UT. An EIT wave transient (see, e.g., Thompson et al. 2000b) was also observed and was found to be in close (projected) spatial coincidence with the Hα wave. No reliable speed could be determined for this EIT wave because of the low image cadence.

Two entirely different approaches are found in the literature for the interpretation of Moreton Hα waves and EIT waves. The first approach assumes that the Moreton wave is the chromospheric trace of an MHD wave (see, e.g., Moreton 1960; Uchida 1968). Such a wave approach has been extended to EIT waves by Wang (2000). This last model accounts for the cospatiality of the EIT and Hα waves found in this study and is also suggested for another event by Thompson et al. (2000b). However, as pointed out by Wang, the model cannot account for the high velocity of the Moreton wave found in this event unless the initial disturbance is a strong super-Alfvenic shock. In this scenario, the propagation of the wave might have lead to further destabilisation and magnetic interactions when it encountered other large- or small-scale coronal magnetic structures. This was previously suggested by Moreton (1960) for, e.g., the destabilisation of filaments.

Khan & Hudson (2000) suggested that the wave causes also the destabilisation of the interconnecting loop structures seen in soft X-rays. This scenario may also explain the appearance of new radio sources at different locations on the solar disk and the illumination of new magnetic loops as accelerated electrons have access to new field lines. The other radio-emitting sites may be due to the reconnection between the large-scale loop systems. This scenario is supported by the observation of radio bursts going down in the solar atmosphere (i.e., drifting to higher frequencies) after the flash phase. Finally, we note that the new radio sources appeared over a large longitudinal and latitudinal range, which may indicate the extent of the CME source region on the solar disk. A similar observation of the rapid development of the latitudinal extent of radio-emitting sources has been discussed for a limb event by Maia et al. (1999) and attributed to loop-loop interactions resulting in large-scale coronal restructuring and ultimately CME formation in a multipolar magnetic system.

The propagation of the blast wave (the Hα wave speed observed in the photospere was 630–790 km s^{-1}) in the corona and its subsequent interaction and destabilisation of other preexisting large-scale magnetic structures presumably leads to the formation of type II–like drifting radio emissions observed in the spectra between 300 and 200 MHz. These frequency-drifting emissions correspond at each frequency to short-duration, fast-moving radio sources (with projected speeds of 830–890 km s^{-1}) that seem to appear at locations in close spatial and temporal coincidence with the extrapolated location of the Hα wave if it had proceeded almost spherically. They could thus result from the interaction of the wave with existing coronal structures linking the different magnetic regions on the disk. This interaction could result in the generation of secondary

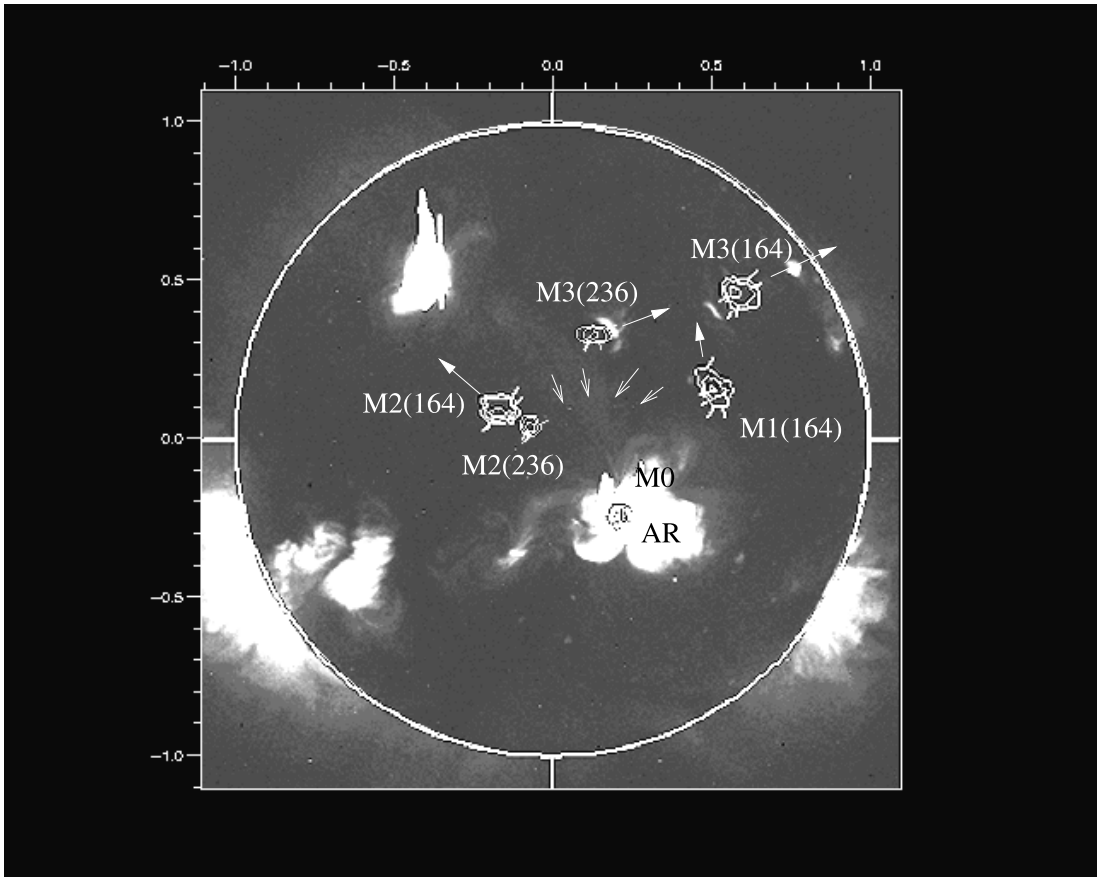

FIG. 13.—Nancay 164 and 236 MHz source locations at selected times showing the moving sources M1 (start time around 13:41 UT), M2 (start time around 13:42 UT), and M3 (start time around 13:42 UT). The active region radio leg is labeled "AR" and the radio flash phase location "M0" (start time around 13:37 UT). The *Yohkoh* SXT preflare gray-scale image is from 13:26 UT on 1998 May 2. The arrows north of the active region point to the locations where the Hα wave front was observed at 13:39:47 UT. The axes units are solar radii.

shock waves leading to the type II–like radiation. The fact that M1 and M3 seem to overlay bright regions seen either in soft X-rays with *Yohkoh* or in EUV with EIT gives some support to such a scenario.

Another interpretation of the EIT waves has been introduced by Delannée & Aulanier (1999). They link the location of the EIT brightening to the result of the compression of the plasma near the footpoints of opening field lines. This bright feature can propagate as the field opens farther and

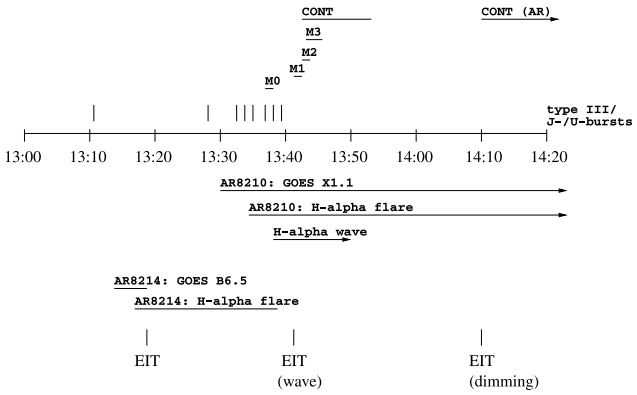

FIG. 14.—Schematic representation of the activity during 13:00–14:10 UT on 1998 May 2.

farther away from the original site. This scenario may also account for the rapid development of the extent of radio-emitting sources on the disk and on the formation of type II–like bursts as the field opening proceeds farther and encounters preexisting magnetic features.

The radio observations provide another signature of the arc expansion of the CME magnetic field and show that around the time of the last spectral drifting feature, large and expanding continuum radio sources were formed (speeds around 300 km s^{-1}). An EIT dimming region was observed later in the same location. This radio continuum emission presumably arises from electrons accelerated in the expanding large-scale loops associated with the CME. Thus, the large radio source as well as the EIT and SXT dimming regions may trace the on-the-disk locations of the CME source regions. In the final phase of the flare, there was no longer evidence for large-scale radio-emitting sources nor for emitting sites spread largely on the disk.

In conclusion, we have presented a multiwavelength analysis of an on-the-disk flare associated with a halo CME event on 1998 May 2. The emphasis was on studying the radio-imaging and spectral data together with soft X-ray, EUV, and Hα data in order to show and understand the rapid development occurring on small and large scales during the flare and CME onset. It must be noted that we did not address in this paper the question of which one of these phenomena triggers the other, but rather we show

that the flare and the CME can each be signatures of the fast evolution of multipolar magnetic fields.

The authors wish to thank G. Aulanier for helpful discussions, H. Hudson for useful comments on the manuscript, and the referee for improving the clarity of the paper. *Yohkoh* is a project of the Institute of Space and Astronautical Science (ISAS) of Japan in cooperation with institutes in Japan, the US, and the UK. It is financially supported by ISAS, NASA, and the Particle Physics and Astronomy Research Council (PPARC) of the UK. *SOHO* EIT was built by an international consortium involving ESA and NASA under the supervision of J. P. Delaboudinière (PI), and *SOHO* LASCO was built by the Naval Research Laboratory (US), the Max Planck-Institut für Aeronomie (Germany), the Laboratoire d'Astronomie Spatiale (France), and the University of Birmingham School of Physics and Astronomy (UK). SOONSPOT data comes from the Solar Observing Optical Network, which includes five solar observatories maintained and operated by the US Air Force. S. P. was supported in Meudon by the Academy of Finland Contract 42576. J. I. K. was supported by PPARC.

REFERENCES

Brueckner, G. E., et al. 1995, Sol. Phys., 162, 357
Cane, H. V., Sheeley, N. R., Jr., & Howard, R. A. 1987, J. Geophys. Res., 92, 9869
Chupp, E. L., Trottet, G., Marschhauser, H., Pick, M., Soru-Escaut, L., Rieger, E., & Dunphy, P. P. 1993, A&A, 275, 602
Cliver, E. W., Webb, D. F., & Howard, R. A. 1999, Sol. Phys., 187, 89
Delaboudinière, J.-P., et al. 1995, Sol. Phys., 162, 291
Delannée, C., & Aulanier, G. 1999, Sol. Phys., 190, 107
Domingo, V., Fleck, B., & Poland, A. I. 1995, Space Sci. Rev., 72, 81
Gopalswamy, N., et al. 1998, J. Geophys. Res., 103, 307
Howard, R. A., Michels, D. J., Sheeley, N. R., Jr., & Koomen, M. J. 1982, ApJ, 263, L101
Hudson, H. S., Lemen, J. R., St. Cyr, O. C., Sterling, A. C., & Webb, D. F. 1998, Geophys. Res. Lett., 25, 2481
Kerdraon, A., & Delouis, J. 1997, in Coronal Physics from Radio and Space Observations, ed. G. Trottet (New York: Springer), 192
Khan, J. I., & Hudson, H. S. 2000, Geophys. Res. Lett., 27, 1083
Klein, K.-L., Khan, J. I., Vilmer, N., Delouis, J.-M., & Aurass H. 1999, A&A, 346, L53
Kosugi, T., et al. 1991, Sol. Phys., 136, 17
Kundu, M. R. 1965, Solar Radio Astronomy (New York: Wiley)
Leblanc, Y., Dulk, G. A., Cairns, I. H., & Bougeret, J.-L. 2000, J. Geophys. Res., 105, 18,215
Maia, D., Pick, M., Vourlidas, A., & Howard, R. 2000, ApJ, 528, L49
Maia, D., Vourlidas, A., Pick, M., Howard, R., Schwenn, R., & Magalhaes A. 1999, J. Geophys. Res., 104, 12,507
Maroulis, D., Dumas, G., Caroubalos, C., Bougeret, J. L., Moussas, X., Alissandrakis, C., & Patavalis, N. 1997, Sol. Phys., 172, 353
Messerotti, M., Otruba, W., Warmuth, A., Cacciani, A., Moretti, P. F., Hanslmeier, A., & Steinegger, M. 1999, in Proc. ESA Workshop on Space Weather (ESA WPP 155; Noordwijk: Netherlands), 321
Messmer, P., Benz, A. O., & Monstein, C. 1999, Sol. Phys., 187, 335
Moreton, G. E. 1960, AJ, 65, 494
Moreton, G. E., & Ramsey, H. E. 1960, PASP, 72, 357
Ogawara, Y., Takano, T., Kato, T., Kosugi, T., Tsuneta, S., Watanabe, T., Kondo, I., & Uchida, Y. 1991, Sol. Phys., 136, 1
Pick, M., Maia, D., Vourlidas, A., Benz, A. O., Howard, R., & Thompson, B. 1999, in AIP Conf. Proc. 417, Solar Wind 9, ed. S. R. Habbal et al. (Woodbury: AIP), 649
Pohjolainen, S., Khan, J., & Vilmer, N. 1999, in Ninth European Meeting on Solar Physics: Magnetic Fields and Solar Processes, ed. A. Wilson (ESA SP-448; Noordwijk: ESA), 205
Raoult, A., Pick, M., Dennis, B. R., & Kane, S. R. 1985, ApJ, 299, 1027
Roberts, J. A. 1959, Australian J. Phys., 12, 327
Sheeley, N. R., Jr., Walters, J. H., Wang, Y.-M., & Howard, R. A. 1999, J. Geophys. Res., 104, 24,739
Sterling, A. C., & Hudson, H. S. 1997, ApJ, 491, L55
Thompson, B. J., Cliver, E. W., Nitta, N., Delannée, C., & Delaboudinière, J. P. 2000a, Geophys. Res. Lett., 27, 1431
Thompson, B. J., et al. 1999, ApJ, 517, L151
Thompson, B. J., Plunkett, S. P., Gurman, J. B., Newmark, J. S., St. Cyr, O. C., & Nichels, D. J. 1998, Geophys. Res. Lett., 25, 2465
Thompson, B. J., Reynolds, B., Aurass, H., Gopalswamy, N., Gurman, J. B., Hudson, H. S., Martin, S. F., & St. Cyr, O. C. 2000b, Sol. Phys., 193, 161
Torsti, J., et al. 1998, Geophys. Res. Lett., 25, 2525
Trottet, G., Vilmer, N., Barat, C., Benz, A., Magun, A., Kuznetsov, A., Sunyaev, R., & Terekhov, O. 1998, A&A, 334, 1099
Tsuneta, S., et al. 1991, Sol. Phys., 136, 37
Uchida, Y. 1968, Sol. Phys., 4, 30
Wang, Y.-M. 2000, ApJ, 543, L89
Warmuth, A., Hanslmeier, A., Messerotti, M., Cacciani, A., Moretti, P. F., & Otruba, W. 2000, Sol. Phys., 194, 103
Zarro, D. M., Sterling, A. C., Thompson, B. J., Hudson, H. S., & Nitta, N. 1999, ApJ, 520, L139
Zharkova, V. V., & Kosovichev, A. G. 1999, in Plasma Dynamics and Diagnostics in the Solar Transition Region and Corona, ed. J.-C. Vial & B. Kaldeich-Schürmann (ESA SP-446; Noordwijk: ESA), 756